Neuron, Vol. 33, 733–747, August 15, 2002, Copyright ©2002 by Cell Press

Mechanisms Regulating Variability of the Single Photon Responses of Mammalian Rod Photoreceptors

Greg D. Field and Fred Rieke[1]
Department of Physiology and Biophysics
University of Washington
Seattle, Washington 98195

Summary

Variability in the single photon responses of rod photoreceptors limits the accuracy with which the number and timing of photon absorptions are encoded. We investigated how much single photon responses of mammalian rods fluctuate and what mechanisms control these fluctuations. Mammalian rods, like those of toads, generated responses to single photons with trial-to-trial fluctuations 3–4 times smaller than other familiar signals produced by single molecules. We used the properties of the measured fluctuations to constrain models for how the single photon responses are regulated. Neither feedback control of rhodopsin's activity nor saturation within the transduction cascade were consistent with experiment. The measured responses, however, could be explained by multistep shutoff of rhodopsin or a combination of multistep shutoff and saturation.

Introduction

We all share the qualitative impression that our sensory systems are precise. Indeed, in a number of instances, sensory performance approaches or reaches fundamental limits set by the physical nature of the sensory inputs themselves (reviewed by Bialek, 1987). Chemotactic bacteria sense concentration gradients with an accuracy that requires counting molecules bound to receptors on their surface (Berg and Purcell, 1977). Just-detectable sounds produce movements of auditory hair cell stereocilia similar in magnitude to those produced by Brownian motion (Bialek, 1987). The dark-adapted visual system can detect and possibly even count the absorption of a few photons (Hecht et al., 1942; Sakitt, 1972; reviewed by Rieke and Baylor, 1998a). Consistent with photon counting, toad rod photoreceptors generate reproducible single photon responses—i.e., responses with nearly constant amplitude and time course—permitting one absorbed photon to be distinguished from two (Baylor et al., 1979b).

Reproducibility of the rod's single photon response is surprising because the response originates from a single light-activated rhodopsin molecule. Most signals from single molecules show large trial-to-trial fluctuations caused by the variable duration of the molecule's active lifetime. A familiar example is the charge flowing through an ion channel during its open time. After opening, a typical ion channel with a single open state has a constant probability per unit time of closing (Hille, 2001). The stochastic lifetimes of such a channel are exponentially distributed, so that the standard deviation of the lifetimes is equal to the mean resulting in a coefficient of variation equal to one.

Trial-to-trial fluctuations in the single photon responses of toad rods are only 20%–25% as large as expected for the termination of rhodopsin's catalytic activity through a single stochastic step (Baylor et al., 1979b; Rieke and Baylor, 1998b; Whitlock and Lamb, 1999). This low variability indicates that fluctuations in rhodopsin's activity are small or that the measured responses are insensitive to such fluctuations. Feedback regulation of rhodopsin's active lifetime (Whitlock and Lamb, 1999) or shutoff through a series of steps (Rieke and Baylor, 1998b) could reduce fluctuations in rhodopsin activity. Saturation within the transduction cascade (Felber et al., 1996) could make the measured responses insensitive to variations in rhodopsin's activity. Rhodopsin is a member of the large family of G protein-coupled receptors which share a common structure and common steps in shutoff (reviewed by Bohm et al., 1997). Thus, the mechanisms responsible for regulating signals from single rhodopsin molecules may more generally permit G protein signaling cascades to produce signals that accurately represent the number of active receptors.

Variability of the single photon response has not been investigated thoroughly in mammalian rods, making it difficult to determine the importance of reproducibility for behavioral sensitivity. Furthermore, the mechanisms responsible for reproducibility are not agreed upon (Rieke and Baylor, 1998b; Whitlock and Lamb, 1999). Here we measure variability in the single photon responses of primate and guinea pig rods and investigate how the variability is regulated. We find that the areas of the single photon responses of mammalian rods have a coefficient of variation 3–4 times smaller than that expected for first-order decay of rhodopsin's activity. We compare the time course and magnitude of the response fluctuations to predictions from three classes of models. No model based on feedback control of rhodopsin shutoff or saturation within the transduction cascade was consistent with the experiment. However, shutoff of rhodopsin's activity through a series of 12–14 steps could explain the properties of the measured responses. The number of steps required could be reduced to 8–10 by combining multistep shutoff and saturation. As a further test, we slowed light-dependent changes in Ca^{2+} by loading cells with BAPTA; this slowed the responses but did not increase their variability. When we accounted for the known action of Ca^{2+} on the transduction cascade, the multistep shutoff model used for the control responses generalized well to account for the variability measured in BAPTA-loaded rods.

Results

Properties of Single Photon Responses

We measured variability of the single photon response by isolating responses to 0 and 1 photoisomerization

[1]Correspondence: rieke@u.washington.edu

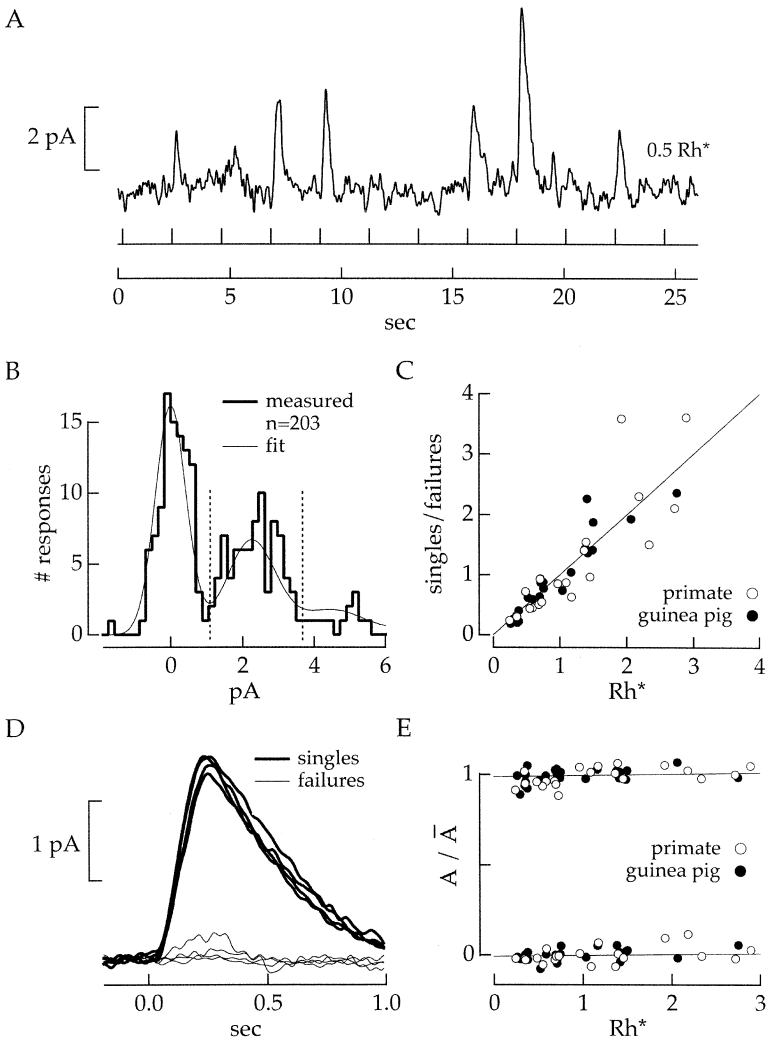

Figure 1. Isolation of Single Photon Responses

(A) Responses of a primate rod to a series of fixed-strength flashes are shown. Dark current was 25 pA; bandwidth was 0–5 Hz.

(B) Amplitude histogram is plotted from the same rod and flash strength as in (A). Vertical dotted lines show thresholds used to identify singles and failures.

(C) Control for systematic bias in isolation is shown. The y axis plots the mean number of Rh* estimated from the ratio of the number of identified singles to failures. The x axis plots the estimate from the flash strength and collecting area. Systematic bias in isolation would cause deviations from the line of unity slope.

(D) Control for contamination in isolated singles and failures is shown. Comparison of the average single and failure isolated from four flash strengths in a primate rod. Contamination would cause the average to depend on flash strength.

(E) Amplitude of the average single and failure is plotted as a function of flash strength. Amplitudes were normalized by the average single amplitude across all flash strengths, $\bar{A}$.

(Rh*) from repeated presentations of a fixed-strength flash. Below we describe the isolation procedure and the characteristics of the variability.

Sources of Variability in the Rod Responses to a Repeated Flash

Both primate and guinea pig rods generated quantized responses to a repeated flash. Figure 1A shows a section of current record from a primate rod stimulated with flashes producing on average 0.5 Rh*. Several sources contributed to trial-to-trial variability in the rod responses. The dominant source was Poisson fluctuations in the number of absorbed photons (Baylor et al., 1979b). Response variability also contained contributions from two cellular noise sources: continuous fluctuations in the baseline current (Baylor et al., 1980) and variations in the single photon response (Baylor et al., 1979b; Rieke and Baylor, 1998b; Whitlock and Lamb, 1999). Instrumental noise made a negligible contribution to the variability (see Experimental Procedures).

We separated each contribution to the trial-to-trial response fluctuations by constructing histograms of the response amplitudes, as in Figure 1B. Amplitudes were measured from the correlation between individual responses and a scaled version of the average response (see Experimental Procedures). The peak in the histogram centered on an amplitude of zero corresponds to the trials in which the cell failed to respond ("failures"). The width of this peak is dominated by the cell's continuous dark noise (Baylor et al., 1980, 1984). The peak centered around 2 pA corresponds to the rod's single photon response ("singles"). The width of this peak includes contributions from variability in the single photon response as well as dark noise.

To measure the variability attributable to the single photon response itself, we isolated singles and failures from histograms like that in Figure 1B. Bias in the isolation procedure will cause systematic overestimates or underestimates of the response variability. Below we describe the isolation procedure and the controls used to check for potential bias.

Isolation of Single Photon Responses

We separated single photon responses from failures and multiphoton responses by fitting the amplitude histograms according to Equation 1 (smooth curve in Figure 1B; see Experimental Procedures for details). The fits provided an estimate of the mean and standard devia-

tion of the single photon response amplitude and the standard deviation of the noise in darkness. We used these parameters to identify responses that contributed to the failures and singles peaks in the histograms. For example, in Figure 1B, responses with amplitudes less than 1.1 pA were identified as failures and responses with amplitudes between 1.1 and 3.4 pA were identified as singles (dotted lines). Each cell was stimulated with flashes of 3–4 strengths and the same criteria were used to isolate singles and failures across flash strengths.

The isolation procedure described above could fail in two ways: (1) systematic bias, e.g., due to thresholds too close together, could cause the identified singles to represent a small subset of the true single photon responses; or, (2) the identified singles could be contaminated with failures or multiphoton responses. Similar errors could occur in identification of failures. The parameters of the histogram fits suggested these errors were small (see Experimental Procedures). We verified this using two tests based directly on the isolated responses, as described below. These tests provided a basis for identifying rods (8 of 10 from primate and 9 of 19 from guinea pig) in which singles and failures could be isolated reliably; subsequent analysis used only these cells. The excluded rods generated single photon responses too small to be separated reliably from dark noise.

We first verified that the number of identified singles and failures agreed with expectations from the Poisson statistics that govern photon absorption. From Poisson statistics, the number of singles divided by the number of failures estimates the mean number of Rh* produced by the flash. Figure 1C compares this ratio to the mean number of Rh* estimated from the cell's collecting area and the flash strength. Collecting areas were estimated separately for each cell (see Experimental Procedures). Each point in Figure 1C represents measurements at a single flash strength from a single cell. The line of unity slope represents the expectation if the number of identified singles and failures behaved in accordance with Poisson statistics. The slope of the best-fit line through the measured points did not differ significantly from this expectation. This indicates that the criteria used to identify singles and failures did not systematically underestimate the number of one type and overestimate the number of the other.

Isolating singles and failures across 3–4 flash strengths from each cell allowed us to test for contamination. Since the criteria for isolation were fixed across flash strengths, contamination would cause the average single or failure isolated from flashes of one strength to differ from the averages for another flash strength. For example, if the identified singles contained many multiphoton responses, the number of these contaminating responses would increase at higher flash strengths, causing the average isolated single to increase in amplitude. Figure 1D shows average singles and failures from four flash strengths for a primate rod. The average failures show little structure at all flash strengths, indicating that they are not substantially contaminated with single photon responses. The average singles are also similar across flash strengths, indicating little contamination from failures or multiphoton responses.

The lack of dependence of the isolated singles and failures on flash strength provided a bound on the extent of contamination. Figure 1E summarizes measures of the average failure and single amplitude as a function of flash strength from eight primate and nine guinea pig rods. Contamination would cause the amplitude of the singles or failures to increase with flash strength as fewer failures and more multiphoton responses occur. Thus contamination would produce a positive slope in the relation between amplitude and flash strength. Results from each cell were fit separately; the average slope of the best-fit line through the measured amplitudes was 0.008 ± 0.015 (mean $\pm$ SD) for the singles and 0.005 ± 0.009 for the failures. This lack of dependence on flash strength indicated that 90%–95% of the identified responses were true single photon responses, with contamination from $<5\%$ failures and $<5\%$ multiphoton responses (see Experimental Procedures). The measures of response variability described below were relatively insensitive to this level of contamination (see Experimental Procedures).

Variability of Single Photon Responses

The analyses of Figures 1C–1E identified a set of rods in which singles and failures could be isolated reliably. We used the isolated responses from these cells to separate variability in the single photon response itself from that due to dark noise. We were particularly interested in the total response variability and how this variability evolved over time, as these measures constrained the underlying mechanisms.

Figure 2A shows 50 superimposed singles and failures from a primate and a guinea pig rod. We quantified the total variability by integrating each single and failure and calculating the mean and standard deviation of the resulting areas. The area captures fluctuations occurring at any time point during the response, and thus provides a good measure of the total extent of response fluctuations. Variations in the areas of the isolated singles contained contributions from dark noise and from fluctuations in the single photon responses. Assuming these noise sources were independent and additive (see below), the variance attributable to the single photon response was obtained by subtracting the variance of the areas of the isolated failures from that of the isolated singles. The coefficient of variation (standard deviation divided by the mean) of the single photon response area was 0.26 ± 0.06 in primate (8 cells; mean $\pm$ SD) and 0.30 ± 0.05 in guinea pig (9 cells). This is much smaller than the coefficient of variation of 1 expected for a process governed by a memoryless first-order process, such as the open-close transition of an ion channel. This low variability provides one constraint on potential models for how fluctuations in the response are controlled.

Variability in the singles in Figure 2A appears greater during the response recovery than during the rising phase, as seen previously in toad rods (Rieke and Baylor, 1998b; Whitlock and Lamb, 1999). The time course of the variations could be seen more clearly by calculating the time-dependent variance. Figure 2B shows the variance of the singles and the failures for the rods of Figure 2A. Assuming independence, subtracting the variance of the singles from that of the failures determines the variance increase attributable to the single photon response. Neither the mean nor the variance of

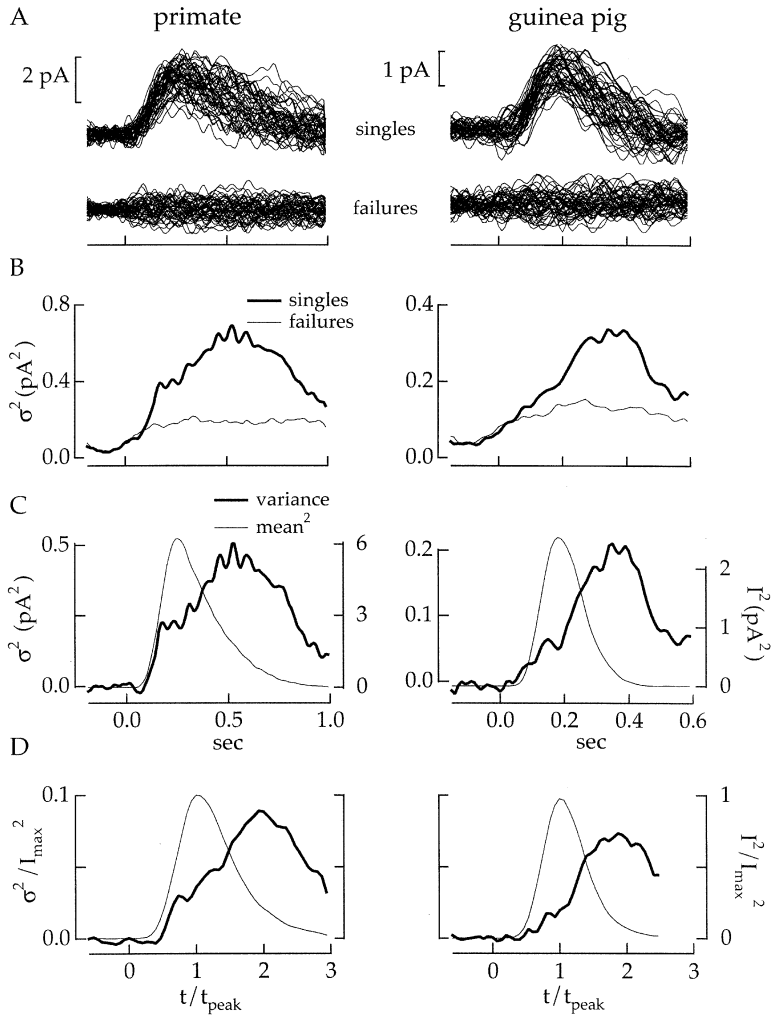

Figure 2. Variability in Single Photon Responses

(A) Collection of 50 isolated singles and failures in a primate and a guinea pig rod are superimposed. Each response has been corrected for changes in the baseline by subtracting the average of a 200 ms window preceding the flash. Dark currents were 25 pA in the primate rod and 18 pA in the guinea pig rod. Bandwidth was 0–20 Hz.

(B) The time-dependent variances of the singles and failures are plotted for the rods in (A).

(C) The variance increase attributable to the single photon response (singles variance—failures variance) and the square of the mean response are superimposed.

(D) The squared mean and variance averaged from eight primate rods and nine guinea pig rods are superimposed. Responses in each cell were normalized by the amplitude and time-to-peak of the cell's average single photon response.

the singles was correlated with the size of the dark noise fluctuation immediately preceding the flash (data not shown), indicating that the dark noise and fluctuations in the singles were indeed independent. The difference variance is shown in Figure 2C along with the square of the mean response. The time course of the variance and the square of the mean differed, with the variance reaching its maximum much later.

To pool data from several rods, we normalized the responses of each cell by the amplitude and time-to-peak of the cell's mean single photon response. We then averaged the mean and variance across cells. Figure 2D plots the square of the mean and the variance of the normalized responses from eight primate and nine guinea pig rods. In rods of both types, the variance of the single photon response takes 1.8 to 1.9 times as long as the mean to peak. The variance also has a broader temporal width than the response itself. The time course of the variance relative to the mean provides a second constraint on models for how the response is regulated.

Mechanisms Limiting Variability in the Single Photon Response

Reproducibility could arise either because variations in rhodopsin's activity are small or because the transduction cascade (Figure 9, reviewed by Arshavsky et al., 2002) renders the measured current responses insensitive to variations in rhodopsin's activity. Rhodopsin acts as a catalyst, activating hundreds or thousands of transducin molecules before shutting off (Vuong et al., 1984; Leskov et al., 2000). Transducin activates phosphodiesterase (PDE), which in turn hydrolyzes cGMP. Rhodopsin, transducin, and PDE all reside on internal membrane discs. Cyclic GMP is a diffusible messenger that relays the activity on the disc to the outer segment membrane where cGMP-gated channels reside. Thus, rhodopsin activation leads to a closure of cGMP-gated channels and a decrease in current. Response fluctuations produced by activation products of rhodopsin are expected to be small because many copies of these molecules contribute to the response.

If the amplifying steps in the transduction cascade operate linearly, the single photon responses will be fully sensitive to variations in rhodopsin's catalytic activity. Alternatively, saturation—e.g., local depletion of transducin or PDE on the outer segment disc, or closure of most or all of the cGMP-gated channels in a local region of the outer segment—could reduce the sensitivity of the response to variations in rhodopsin's activity. Below we test each possibility.

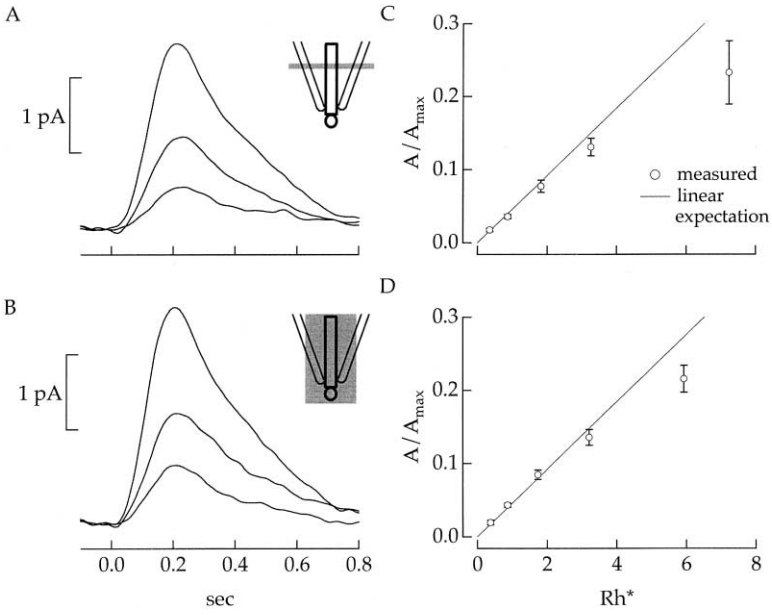

Figure 3. Linearity of Rod Responses to Local and Uniform Illumination

(A) Responses of a guinea pig rod to local illumination are plotted. Responses to flashes producing on average 0.75, 1.5, and 3 Rh* restricted to a 1–2 μm strip of the outer segment are superimposed. Dark current was 19 pA; bandwidth was 0–10 Hz.

(B) Responses of the same cell to uniform illumination are plotted. Responses to flashes producing on average 0.95, 1.9, and 3.8 Rh* are superimposed.

(C) Measurements of the dependence of the response amplitude on flash strength for local illumination are summarized. Amplitudes were normalized by the cell's maximum responses and averaged across cells. These normalized amplitudes are plotted against the flash strength. Data points are mean ± SEM from 10 guinea pig rods. The straight line was fit to the lower 3 points and has a slope of 0.046/Rh*.

(D) Measurements for diffuse illumination are summarized. The straight line is identical to that in (C).

Local Depletion of cGMP or Open cGMP-Gated Channels

If the single photon response significantly depleted cGMP or open cGMP-gated channels near the site of photon absorption, the response to two absorbed photons falling in the same region of the outer segment should be less than twice the single photon response. To test for such a saturation, we delivered dim flashes that either illuminated the entire outer segment or were restricted to a narrow transverse strip. Since the single photon response decreased the outer segment current by about 5%, the response affected at least a 1.25 μm wide region of the ~25 μm long outer segment. Our spatially restricted stimuli fell on a 1–2 μm wide region of the outer segment (see Experimental Procedures). Since this region contained about 40 internal discs, these experiments tested the sensitivity of the membrane current to local activity of multiple discs rather than saturation of the reactions occurring on a single disc.

Figure 3 shows average responses of a guinea pig rod to dim flashes of 3 different strengths delivered either locally (Figure 3A) or uniformly (Figure 3B). The increase in response amplitude with increasing flash strength was similar in each case. Figures 3C and 3D show average results from ten guinea pig rods. Responses to both uniform and local illumination summed nearly linearly up to 3 Rh*. Furthermore, the response per Rh* was essentially identical for the two stimuli (the straight lines in Figures 3C and 3D are the same). Primate rods also responded similarly to spatially restricted and uniform dim flashes (seven cells; data not shown).

The results of Figure 3 indicate that signals produced by multiple photons absorbed within a 1–2 μm wide region of the outer segment did not interact strongly. Thus, depletion of cGMP or cGMP-gated channels did not significantly affect the single photon response. This conclusion held even if the spatially restricted stimuli illuminated a larger region of the outer segment than our calibrations suggest (see Experimental Procedures). Thus, we turned to other possible explanations for reproducibility.

Other Models: Feedback, Depletion of Transducin or PDE, and Multistep Shutoff

The experiments described above indicate that the low variability of the single photon response is caused by events on the membrane disc rather than the machinery coupling the disc to the membrane current. Insensitivity of the activity on the disc to variations in rhodopsin's activity could occur through depletion of transducin or PDE (Figure 4A). Alternatively, variability in rhodopsin's activity could be small due to feedback (Figure 4B) or to shutoff through a series of steps (Figure 4C). Each of these possibilities defines a class of models. We identified the particular model of each class that best captured the measured magnitude and time course of the response variability. Multistep shutoff of rhodopsin's activity was the single mechanism most consistent with experiment. We consider combinations of mechanisms in the Discussion.

The first class of models involved depletion of the pool of available transducin or PDE (Figure 4A). Rhodopsin shutoff was described as a single first-order reaction. While rhodopsin was active, the available transducin or PDE was gradually depleted. This caused the effective catalytic activity—the rate at which rhodopsin activated transducin and PDE—to decline exponentially with time following photon absorption. The lowered effective catalytic activity decreased the sensitivity of the responses to variations in rhodopsin's lifetime because amplification was low by the time rhodopsin shut off. A simulated single photon response was produced by passing the effective catalytic activity through a deterministic filter representing the action of the transduction cascade (see Experimental Procedures). Trial-to-trial response variability in this model was determined by the rate of decline in effective catalytic activity, with a large rate of decline causing less variability.

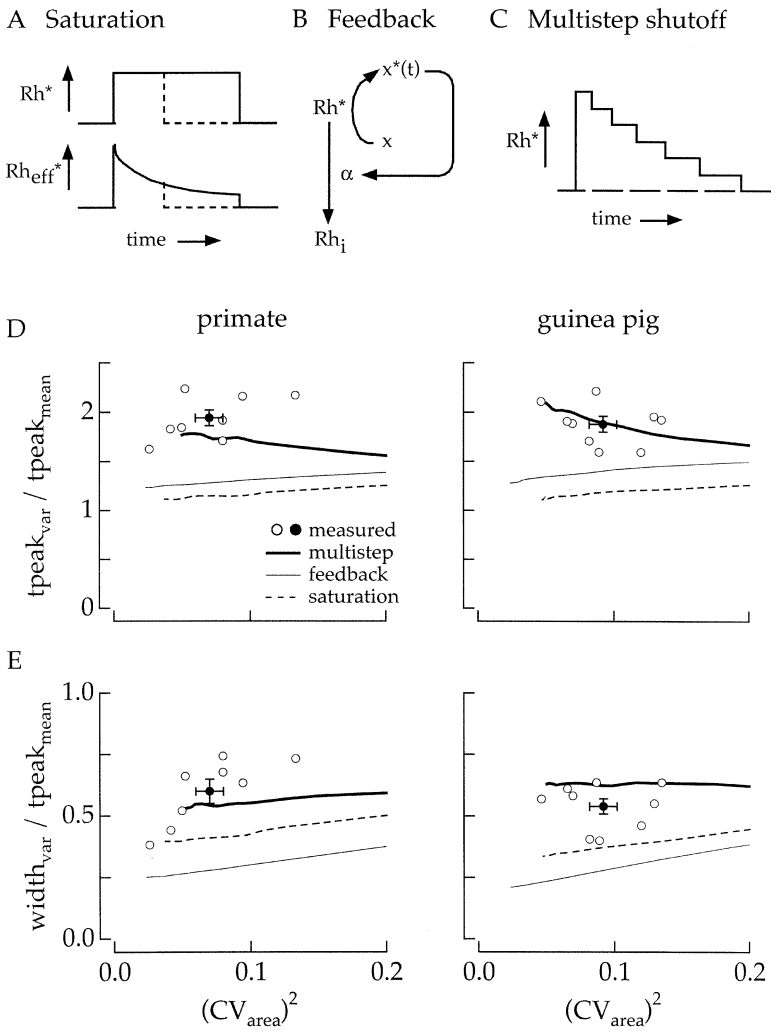

Figure 4. Comparison of Predicted and Measured Fluctuations in the Single Photon Response

(A–C) Three mechanisms are capable of decreasing variability in the single photon response: saturation within the transduction cascade, feedback regulation of rhodopsin shutoff, and shutoff through a series of steps. Each mechanism has a single parameter that controls the response variability; changing this parameter generated a series of predictions that we compared with experiment.

(D) The time-to-peak of the variance relative to that of the mean is plotted against the square of the coefficient of variation of the response areas. Open circles show data from individual cells; the filled circle is the mean with error bars showing the SEM.

(E) The temporal width of the variance relative to the time-to-peak of the mean is plotted against variability in the response areas. The width was defined as the standard deviation of a Gaussian fit to the measured variance.

The second class of models we considered was control of rhodopsin shutoff by feedback from a downstream activation product of rhodopsin (Figure 4B). The time course of the activity of a single rhodopsin molecule was generated from a stochastic model in which the rhodopsin shutoff rate was subject to feedback signal x that accumulated linearly in time and acted with a cooperativity h. This feedback caused the shutoff rate, α, to increase as t^h, and this increase in shutoff rate over time decreased variability in rhodopsin's active lifetime. The feedback signal started from an initial value of 0 because this produced the largest decrease in variability. The rate at which the feedback signal increased was set to produce an average rhodopsin lifetime near 200 ms. The cooperativity in this model could account for nonlinear changes in the feedback signal itself or a nonlinear action of the feedback signal on rhodopsin shutoff. This model assumes only that the feedback originates downstream of rhodopsin and thus includes Ca^{2+}-dependent and Ca^{2+}-independent feedback. Single photon responses were generated as above. The cooperativity of the feedback signal determined the trial-to-trial response variability in this model; variability in the responses decreased as the cooperativity increased.

In the third class of models, rhodopsin shutoff was described by a series of n steps or transitions (Figure 4C), each of which produced the same decrease in activity. The largest reduction in variability was obtained when each step controlled the same fraction of rhodopsin's cumulative activity. To achieve this, the transition rates between steps were scaled so that the first transition had a rate constant of $n\alpha$, the second $(n-1)\alpha$, and so on. Increasing the number of steps in shutoff decreased variability because the cumulative rhodopsin activity scaled with the number of steps while the standard deviation scaled as the square root of the number of steps. Thus, the coefficient of variation scaled as $1/\sqrt{n}$. Simulated responses were generated as above.

Each class of models made different predictions about the magnitude and time course of the fluctuations in the single photon response. Figures 4D and 4E compare these predictions with experiment. For each class of models, we varied the parameter controlling the variability of the response—the rate of decline of the effective catalytic activity in the saturation models, the cooperativity in the feedback models, and the number of steps in the multistep shutoff models. Each model was constrained to replicate the time course of the average single photon

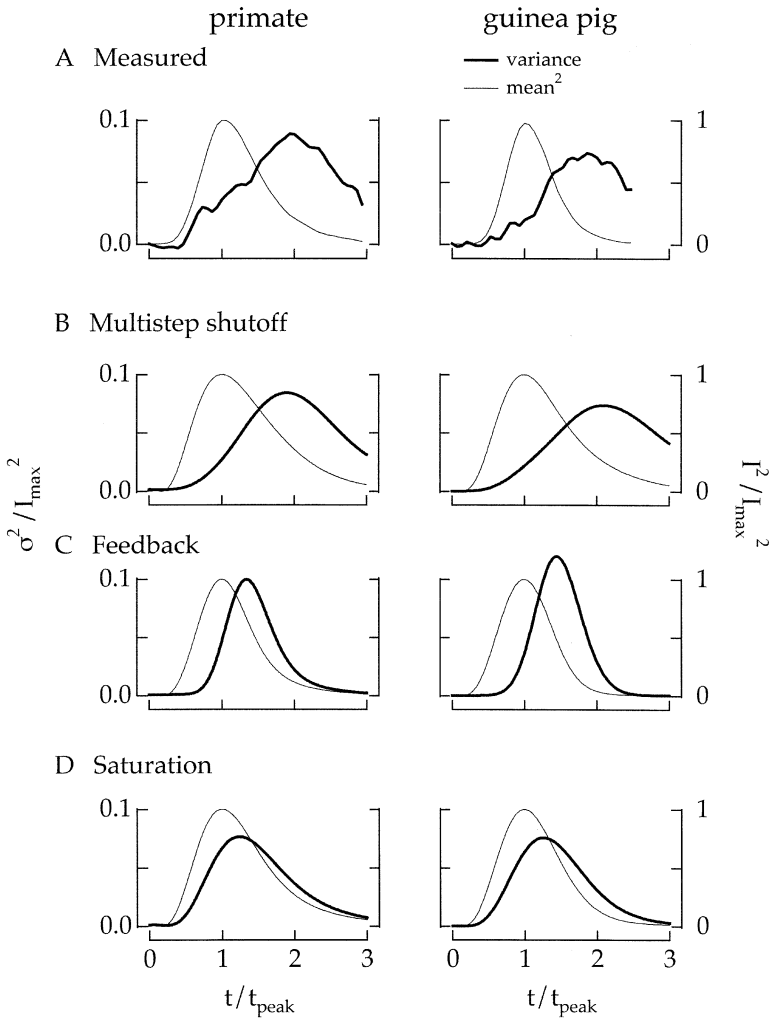

Figure 5. Comparison of Squared Mean and Variance of the Single Photon Response with the Best Instantiation of Each Class of Models

Parameters for each model were determined from Figure 4 as described in Results.
(A) Measured squared mean and variance are plotted.
(B) Multistep shutoff models with 14 (primate) and 12 (guinea pig) shutoff steps are shown.
(C) Feedback models with cooperativities of 3 are shown.
(D) Saturation models with saturation rates of 12 per second are shown.

response (see Experimental Procedures). We compared the predictions each class of models made about three parameters: (1) the square of the coefficient of variation of the response areas; (2) the time-to-peak of the variance relative to that of the mean response; and (3) the temporal width of the variance relative to the time-to-peak of the mean. Figure 4D plots the time-to-peak of the variance against the variability of the response area. Figure 4E plots the width of the variance against the variability of the response area. Each model was able to reduce the variability in response area to measured levels. However, only the multistep shutoff model was able to do so while also capturing the time-to-peak and width of the variance.

The analysis described above identified the model of each class that best captured the data—i.e., the model that minimized the mean square error between prediction and experiment across the three parameters in Figures 4D and 4E. Figure 5 shows the square of the mean and the time-dependent variance for the best of each class of models. The late time-to-peak and broad temporal width of the measured variance provided a clear basis for distinguishing the different models. The multistep model separated the time at which rhodopsin began to shut off from the time at which variability in rhodopsin activity peaked. As a consequence, this model captured the time course and magnitude of the variance. The feedback model failed to replicate the time course of the variance. Reducing the variance to the measured level required a feedback cooperativity of ~3. However, this cooperativity caused rhodopsin to shut off in a narrow time window near the peak of the response. Hence the variance in this model peaked earlier and more sharply than measured. The saturation model suffered a similar problem. The decline in rhodopsin's effective catalytic activity due to transducin or PDE depletion had to occur relatively early in the response to reduce the variance to the measured levels; this rapid onset of saturation caused the variance to peak earlier than measured.

The results of Figures 4 and 5 indicate that multistep shutoff is the single mechanism that best accounts for the measured fluctuations in the single photon response. We consider combinations of mechanisms in the Discussion.

Further Tests of Models: Single Photon Responses in BAPTA-Loaded Rods

We tested how well feedback and multistep shutoff models accounted for variability in the single photon

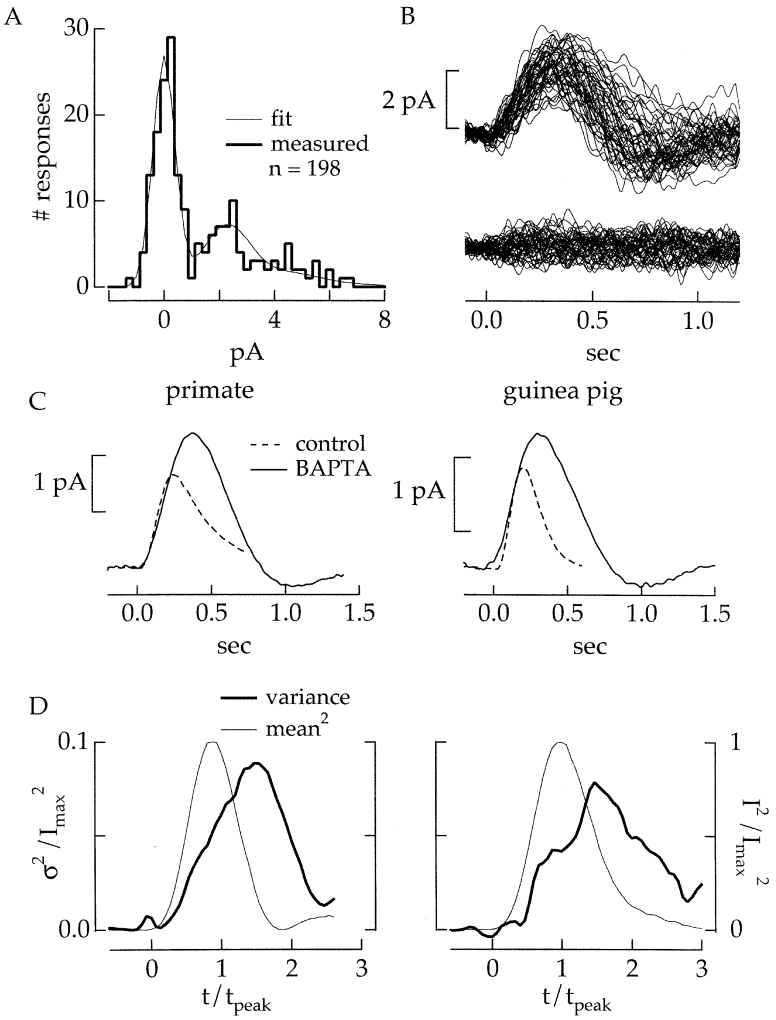

Figure 6. Single Photon Responses from BAPTA-Loaded Rods

(A) An amplitude histogram for responses to a dim flash in a BAPTA-loaded guinea pig rod is plotted.

(B) Collection of 50 isolated singles and failures from the same rod as (A) are superimposed. Dark current was 15 pA and bandwidth was 0–20 Hz. Responses were isolated as in Figure 1.

(C) The mean single photon responses in BAPTA-loaded and control rods are compared (primate: 7 control, 3 BAPTA; guinea pig: 9 control, 3 BAPTA).

(D) The square of the mean and the time-dependent variance of the single photon response are compared for 3 primate and 3 guinea pig rods. To pool data across rods, the responses in each cell were normalized by the time-to-peak and peak amplitude of the average single.

responses when light-induced changes in Ca^{2+} were slowed. These experiments tested directly for a role of Ca^{2+} feedback in regulating rhodopsin shutoff. They also tested how well the multistep model generalized when the properties of phototransduction were changed.

Ca^{2+} provides a feedback signal regulating the kinetics of the light response through its action on the rate of cGMP synthesis (Koch and Stryer, 1988; Mendez et al., 2001; Figure 9). It has also been suggested that Ca^{2+} regulation of rhodopsin shutoff may explain the low variability of the single photon response (Whitlock and Lamb, 1999). If this is the case, slowing light-induced changes in Ca^{2+} should slow the single photon response and increase its variability. If rhodopsin shutoff is not regulated by Ca^{2+} feedback, changes in the single photon response should be fully explained by the slowing in kinetics of the transduction cascade.

Light-induced changes in Ca^{2+} were slowed by loading rods with the Ca^{2+} buffer BAPTA (see Experimental Procedures). Figure 6A shows a histogram of the response amplitudes to a series of fixed-strength flashes from a BAPTA-loaded guinea pig rod. Figure 6B superimposes singles and failures from this cell, isolated as in Figure 1. BAPTA substantially slowed the response kinetics, as shown in Figure 6C. Figure 6D shows the square of the mean and the time-dependent variance for three primate and three guinea pig rods. In each cell, the variance of the failures has been subtracted from that of the singles to isolate the variance attributable to the single photon response. The amplitude and time course of the variance relative to the mean are similar to those under control conditions (Figure 2). Furthermore, the average coefficient of variation of the response areas in BAPTA-loaded rods was 0.27 in primate and 0.2 in guinea pig, not significantly different than in control rods. Thus BAPTA slowed the kinetics of the transduction cascade but did not increase variability of the single photon response.

We next determined how well multistep and feedback models accounted for the shape of the variance under BAPTA-loaded conditions (Figure 7). We used parameters identical to those in Figure 5 except for the rate constant describing Ca^{2+} control of cGMP synthesis (β in Equation 2), which was determined by measuring the Na^+/K^+, Ca^{2+} exchange current (see Experimental Procedures, Figure 9). If Ca^{2+} acts primarily on cGMP synthesis, then changing this rate constant should be sufficient to account for differences between responses in

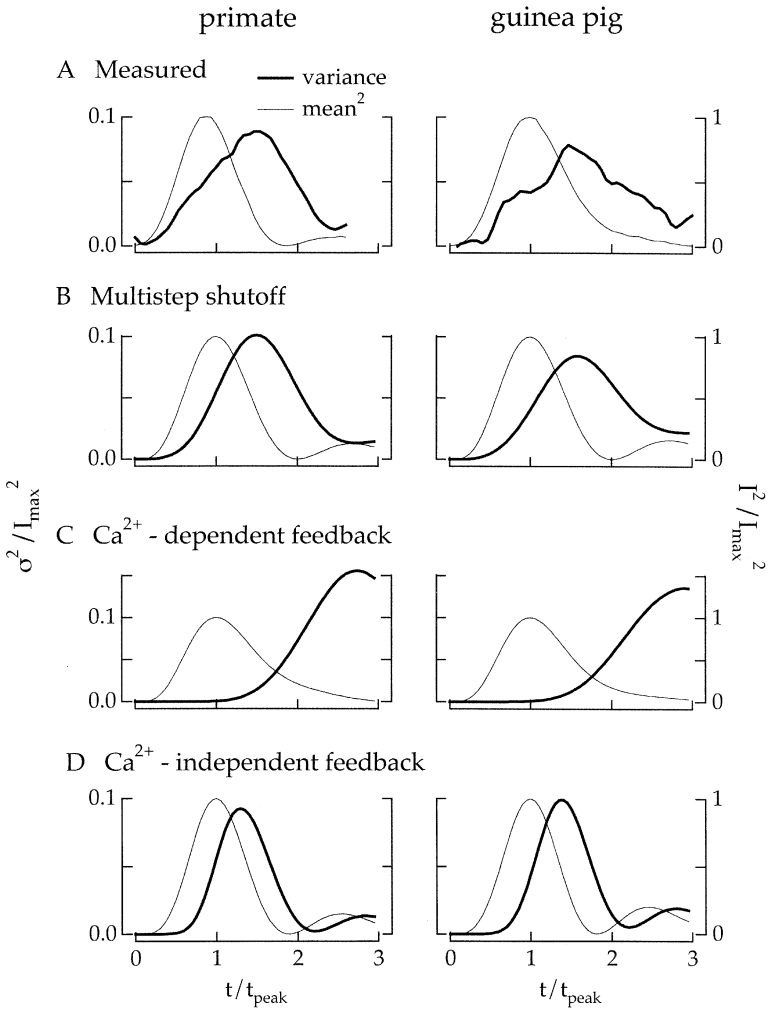

Figure 7. Measured and Predicted Variability in BAPTA-Loaded Rods

Parameters for each model were the same as those in Figure 5 except the Na^+/K^+, Ca^{2+} exchange rate, which was measured as in Figure 9 and altered accordingly in the transduction cascade model (see Equation 1).

(A) Measured squared mean and variance are plotted.

(B) Multistep shutoff models with 14 (left) and 12 (right) steps are shown.

(C) Ca^{2+}-dependent feedback models with cooperativities of 3 are shown.

(D) Ca^{2+}-independent feedback models with cooperativities of 3 are shown.

control and BAPTA-loaded cells. If Ca^{2+} also regulates rhodopsin's lifetime, then changing this rate constant alone should not account for the differences.

Both Ca^{2+}-dependent and Ca^{2+}-independent feedback models failed to account for the measured variance in BAPTA-loaded cells. In the Ca^{2+}-dependent model, the rate of accumulation of the feedback signal *x* was altered according to each rod's measured Na^+/K^+, Ca^{2+} exchange rate. Thus, if BAPTA slowed the exchange rate by a factor of five compared to control conditions, the accumulation of the feedback signal was slowed by the same factor. The light-dependent decrease in Ca^{2+} can lead to the accumulation of a feedback signal (as in Figure 4B) if Ca^{2+} inhibits the feedback. Models were run separately using each experimental cell's measured Na^+/K^+, Ca^{2+} exchange rate and corresponding feedback rate. The resulting variance and squared mean were normalized and averaged. The variance predicted by this model was larger and peaked later than observed (Figure 7C). This is because slowing the light-induced fall in Ca^{2+} prolonged rhodopsin's activity in this model, causing many large and slow single photon responses. In the Ca^{2+}-independent feedback model, only the rate constant for Ca^{2+} control of cGMP synthesis was changed. The variance predicted by this model peaked earlier and had a narrower temporal width than the measured variance (Figure 7D), discrepancies similar to those under control conditions (Figure 5C).

The multistep shutoff model was able to account for the amplitude and time course of the variance under both control and BAPTA-loaded conditions. Figure 7B shows the predicted squared mean and variance for this model. The parameters in Figure 7B are identical to those in Figure 5B except for the rate constant describing Ca^{2+} control of cGMP synthesis, which was measured in each cell as in Figure 9. The multistep model could account for the fluctuations in the single photon response in control and BAPTA-loaded cells without requiring the variations in rhodopsin's activity to change. From this analysis we conclude that the single mechanism that best accounts for the fluctuations in the single photon response under control and BAPTA-loaded conditions is shutoff of rhodopsin through a series of steps.

Discussion

We studied fluctuations in the single photon responses of guinea pig and primate rods. Mammalian rods, like

those of toads, generated responses that varied little in amplitude and shape. This reproducibility permits the rods to encode accurately the time and number of photon absorptions, and may be an important determinant of the behavioral fidelity of rod vision (Rieke and Baylor, 1998b). Reproducibility also poses an interesting molecular design problem as the fluctuations in the single photon response are much smaller than those of other familiar signals controlled by a single molecule, such as the charge flowing through an ion channel during its open time (Hille, 2001). In principle, reproducibility could be conferred by saturation within the phototransduction cascade, by feedback regulating rhodopsin shutoff, or by decay of rhodopsin's activity through a series of steps. We discuss evidence for or against each of these mechanisms below, as well as considering which combinations of mechanisms are consistent with the experiment.

Previous Studies of Reproducibility

Two previous studies analyzed variability in the single photon responses of toad rods (Rieke and Baylor, 1998b; Whitlock and Lamb, 1999). Both found that the responses varied substantially less than expected for shutoff of rhodopsin through a single stochastic step. These studies disagreed, however, on the mechanisms responsible. Rieke and Baylor (1998b) suggested that reproducibility was conferred by shutoff of rhodopsin through a series of 10–20 steps. They rejected a Ca^{2+}-dependent feedback based on dim flash responses measured with changes in internal Ca^{2+} suppressed. Histograms of the response amplitudes under these conditions showed little increase in variability when compared with control histograms. Furthermore, the time-dependent variance of the ensemble of flash responses had a shape similar to the square of the mean response, indicating that Poisson fluctuations provided a larger source of variability than fluctuations in the single photon response.

Whitlock and Lamb (1999) rejected two assumptions made in the interpretation of Rieke and Baylor's constant Ca^{2+} experiments: (1) that amplitude histograms capture the single photon response variations; and (2) that a comparison between the ensemble variance and the square of the mean can identify subtle variability in the single photon response. Instead, Whitlock and Lamb fit their single photon responses with a model that allowed the catalytic lifetime of rhodopsin to vary, but fixed the shutoff of the other components of the transduction cascade. Using this procedure, they estimated the distribution of rhodopsin lifetimes. Repeating this analysis on single photon responses from BAPTA-loaded rods, they observed an increase in the estimated mean lifetime of rhodopsin's activity. This led to the suggestion that Ca^{2+} feedback regulated rhodopsin shutoff.

Two issues complicate interpretation of Whitlock and Lamb's experiments. First, responses of BAPTA-loaded rods should show slow kinetics independent of Ca^{2+} feedback to rhodopsin shutoff because Ca^{2+} regulation of cGMP synthesis plays an important role in accelerating response recovery (Figure 9). If the light-induced fall in Ca^{2+} also provides a feedback speeding rhodopsin shutoff, then the response slowing in BAPTA-loaded rods should be greater than that expected from the slowed feedback to cGMP synthesis. Whitlock and Lamb did not show this because they did not indepen-

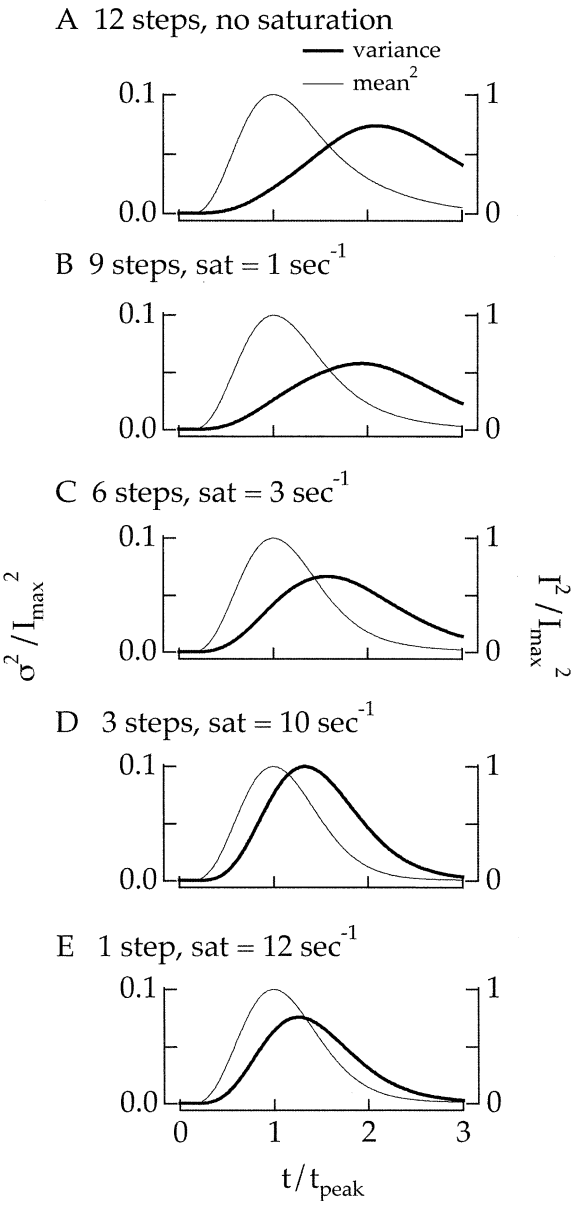

Figure 8. Hybrid Multistep Shutoff and Saturation Model

Each panel plots the squared mean and variance for a model with a different number of steps and different saturation rate. The multistep and saturation models were implemented as in Figure 4. Saturation rates were chosen to provide the best fits to experiment as in Figure 4.

(A) Multistep model with 12 shutoff steps and no saturation is shown.

(B) Model with 9 shutoff steps and a saturation rate constant of 1 s^{-1} is shown.

(C) Model with 6 shutoff steps and a saturation rate constant of 3 s^{-1} is shown.

(D) Model with 3 shutoff steps and a saturation rate constant of 10 s^{-1} is shown.

(E) Model with 1 shutoff step and a saturation rate constant of 12 s^{-1} is shown.

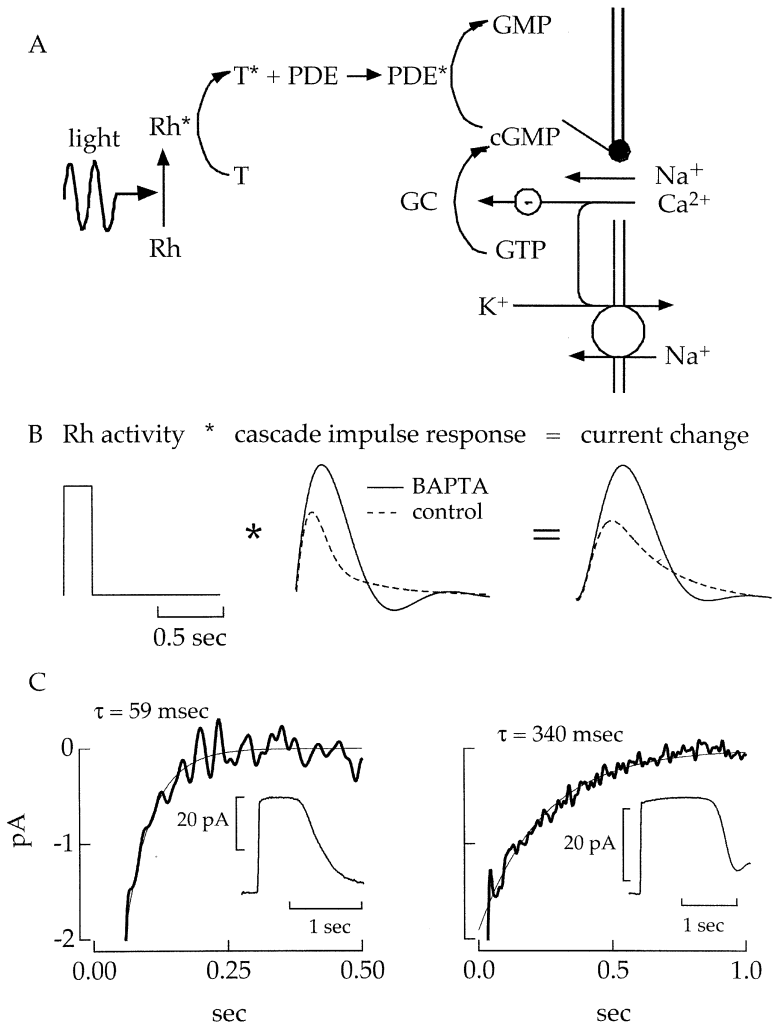

Figure 9. Model for Phototransduction Cascade

(A) The phototransduction cascade is summarized. Photon absorption converts rhodopsin (Rh) to its active form (Rh*). Activated rhodopsin catalyzes activation of the G protein, transducin (T), which then activates phosphodiesterase (PDE). PDE hydrolyzes cGMP, causing membrane channels to close and the current to decrease. The cGMP level is restored by synthesis by guanylate cyclase (GC), the rate of which is regulated by Ca^{2+}. Light causes a decrease in Ca^{2+} influx, while Ca^{2+} efflux through the Na^+/K^+, Ca^{2+} exchanger continues. The resulting drop in Ca^{2+} increases the synthesis rate.

(B) The procedure for simulating single photon responses is illustrated. The time course of rhodopsin activity (left) is passed through a filter describing the transduction cascade (middle) to predict the current change (right). This procedure is shown for control and BAPTA-loaded conditions.

(C) Measurements of the Na^+/K^+, Ca^{2+} exchanger time constant in control and BAPTA-loaded primate rods are shown. Exposure to bright flash rapidly closed the cGMP channels, leaving a small current due to electrogenic Na^+/K^+, Ca^{2+} exchange. The exchange current was fit with a single exponential to estimate the exchanger rate constant. The inset shows the average response.

dently measure the slowing in the response and that in Ca^{2+} kinetics. Thus the inferred increase in rhodopsin lifetime in BAPTA-loaded rods could instead have been caused by a slowed Ca^{2+} feedback to cGMP synthesis. Second, the coefficient of variation in rhodopsin's estimated lifetime in BAPTA-loaded cells was similar to that in control cells, not greater as might be expected if Ca^{2+} feedback acted to suppress variability. Despite its simplicity, it is not clear that feedback control of rhodopsin's lifetime accounts for reproducibility.

Constraints Imposed by Time-Dependent Variance

Our investigation of how reproducibility is achieved differs in one essential way from previous work: the time course of the variance in the single photon response is used to constrain possible mechanisms. The salient property of the variance is that it peaks much later than the mean response and is spread over a considerable time period. Feedback, saturation, and multistep shutoff all decreased the variability, but multistep shutoff was the only single mechanism that captured the shape of the time-dependent variance. This observation generalized to BAPTA-loaded conditions, as the change in the time course of the responses could be attributed to the known action of Ca^{2+} on the rate of cGMP synthesis. The BAPTA experiments were inconsistent with a model incorporating a Ca^{2+} feedback to rhodopsin, as the measured change in Ca^{2+} kinetics predicted a large change in the shape of the variance relative to the mean while none was observed (Figure 7C). More direct evidence against a Ca^{2+} feedback regulating rhodopsin shutoff comes from recent experiments on transgenic mouse rods in which cGMP synthesis was insensitive to Ca^{2+} (Burns et al., 2002). In these rods, dim flash responses were not significantly altered when Ca^{2+} changes were slowed with BAPTA.

The feature that distinguishes multistep shutoff from saturation and feedback is that it allows the response to begin to recover before variations in rhodopsin's activity have reached a peak. This allows multistep shutoff to capture both features observed in the data, a broad time-dependent variance and a late peak. Saturation reduces the gain of transduction when the duration of rhodopsin's activity significantly exceeds the average. This eliminates large, slow responses but causes the peak in the variance to occur far earlier than observed. Feedback reduces the variance to the observed levels

only if rhodopsin is forced to shut off in a narrow time window. This makes the variance peak earlier and have a smaller width than observed.

Can Combinations of the Different Models Account for the Observed Variability?

The single model that agreed most closely with experiment was shutoff of rhodopsin through 12–14 steps. Attributing reproducibility to a single mechanism, however, may be too simplistic. Thus we investigated whether the number of steps could be reduced by combining different mechanisms.

Combining feedback with multistep shutoff failed to reduce the number of necessary steps. A single feedback signal regulating a collection of shutoff steps could optimize the transition rates from one step to the next, such that each step controls an equivalent fraction of rhodopsin's cumulative activity. This equal partitioning of the cumulative activity among steps produces the largest reduction in response fluctuations for a given number of steps. However, these transition rates were already set to minimize variability in our multistep model, and hence feedback conferred no additional benefit.

Combining saturation and multistep shutoff, however, could reduce the number of necessary steps. Figure 8 illustrates the predicted relationship between the squared mean and the variance using different combinations of multistep shutoff and saturation. The agreement between prediction and experiment degrades as the number of steps decreases. The 9-step model of Figure 8B captured the measured response properties in Figure 4 nearly as well as the 12-step model. The 6-step model of Figure 8C was more than 100 times less likely given the error bars on the measurements in Figure 4.

The number of steps determined in this analysis is a lower bound, as fluctuations in rhodopsin's activity would need to be even smaller if there is variability in the transduction cascade. Such variability could arise either from stochastic fluctuations in the activity of its elements or from spatial heterogeneity in their concentrations (Detwiler et al., 2000).

Possible Sources of Multiple Steps

Several events could contribute to multistep shutoff of rhodopsin. Rhodopsin shutoff involves phosphorylation by a kinase followed by the binding of arrestin (Bennett and Sitaramayya, 1988; Palczewski et al., 1992; Chen et al., 1995; Xu et al., 1997). The binding of rhodopsin kinase could be a first step in rhodopsin shutoff, although there is evidence that this binding alone has little effect on rhodopsin's catalytic activity (Mendez et al., 2000). Rhodopsin has six to nine potential phosphorylation sites (Wilden and Kühn, 1982), and the affinity of transducin binding decreases as these sites are phosphorylated (Gibson et al., 2000). Mendez et al. (2000) found that the variability in the single photon response increased in mouse rods with fewer than three sites, and that all six sites in mouse were needed for normal response kinetics. Furthermore, the variability they estimated in wild-type mouse rods is approximately three times greater than that we find in primate and guinea pig rods. This discrepancy may be because they were not able to isolate single photon responses, and hence had to use a less direct estimate of the response variability. Thus, it is possible that each phosphorylation site helps reduce variability.

Molecular Constraints Imposed by Reproducibility

Several conditions must be met for a multistep shutoff process to be effective in reducing variability. First, each step should control a similar fraction of the molecule's total catalytic activity. If one step were to control most of the activity, variability in that step would limit reproducibility. This condition can be met if shutoff involves n independent and equally probable events that can occur in any order, and each event produces the same decrease in activity. Upon activation of the molecule, n possible events can lead to a lower activity state, creating a rate constant n times that of the single event. After each transition, the number of available events decreases, causing the rate constant to slow.

The second condition for multistep shutoff to be effective is that the steps have a much larger forward than reverse rate constant. Reverse transitions will introduce additional variability in the shutoff process and hence require more steps to achieve the same degree of reproducibility. Thermal fluctuations and the decline in free energy produced by each step determine the ratio of forward and reverse rate constants. For shutoff through a series of 10 steps, reproducibility is relatively unaffected by reverse transitions provided the reverse rate constant is at least 20 times smaller than the forward rate constant. This requires a free energy difference of 1.8 kcal/mol. Thus if reproducibility is achieved through a 10 step shutoff process, the free energy difference between fully activated and inactivated—i.e., phosphorylated and arrestin bound—rhodopsin must be at least 18 kcal/mol.

Rhodopsin is one of a large family of G protein-coupled receptors. Similar signaling cascades operate in olfactory (reviewed by Firestein, 2001) and pheromone (reviewed by Dohlman, 2002) receptors, and both of these chemosensory systems can detect a small number of molecules (DeVries and Stuiver, 1961; Menini et al., 1995; Leinders-Zufall et al., 2000). Regulation of receptor activity through a series of shutoff steps could, in principle, improve sensitivity of these systems just as it seems to in vision. For this to be an effective strategy, the receptors themselves would have to satisfy the constraints outlined above: partitioning of the total receptor activity equally among steps, and a large free energy difference between the active and inactive receptors.

Experimental Procedures

Measurements of Rod Photocurrents

We recorded from guinea pig (*Cavia porcellus*) and primate (*Macaca fascicularis* and *Papio anubis*) rods. In guinea pig experiments, an animal was dark adapted overnight, sedated with ketamine (50 mg/kg) and xylazine (5 mg/kg), and killed with an overdose of nembutal (90 mg/kg), following procedures approved by the Administrative Panel on Laboratory Animal Care at the University of Washington. After full anesthesia was achieved, the eyes were enucleated and the retinas isolated. All procedures were carried out under infrared light (>900 nm) to keep the retina fully dark adapted. Isolated retinas were stored in oxygenated Hepes-buffered Ames solution (Sigma, St. Louis, MO) in a light-tight container on ice. In experiments on

primate rods, we obtained a piece of light-adapted retina attached to the choroid and pigment epithelium from Dennis Dacey's laboratory through the Tissue Distribution Program of the Regional Primate Research Center at the University of Washington. The retina was allowed to dark adapt for >1 hr at 37°C in bicarbonate-buffered Ames solution equilibrated with 5% CO_2/95% O_2. Pieces of retina that did not adhere well to the pigment epithelium were discarded and the remaining tissue was stored on ice. No differences were observed between macaque and baboon rods.

Rod outer segment currents were recorded with suction electrodes (Baylor et al., 1979a; Field and Rieke, 2002). Most recordings were from cells protruding from small pieces of retina. During recording, cells were superfused with bicarbonate-buffered Ames solution warmed to 36.5°C–37.5°C. Current collected by the suction electrode was amplified, low-pass filtered at 30 Hz (8 pole Bessel), and digitized at 1 kHz. Responses to saturating and half-saturating flashes were measured periodically to check for stability. At the end of a recording, instrumental noise was isolated by exposing the cell to a bright light that eliminated the outer segment current. Only recordings in which cellular dark noise exceeded instrumental noise were used.

In some experiments, rods were loaded with BAPTA to slow the Ca^{2+} kinetics. A piece of retina was placed in a solution containing 50 μM BAPTA-AM for 20–30 min at 37°C before recording. Successful BAPTA incorporation was indicated by slow biphasic dim flash responses (Matthews, 1991). The time constant for Na^+/K^+, Ca^{2+} exchange was measured in each BAPTA-loaded rod by exposing the cell to saturating flashes that eliminated the outer segment current for 1–2 s. BAPTA incorporation slowed the exchange time constant by a factor of ~6 on average.

Flashes were delivered from a light-emitting diode (LED) with a peak output at a wavelength of 470 nm. All flashes were 10 ms in duration. The LED illuminated a circular area 580 μm in diameter centered on the recorded cell. Photon densities (in photons μm^{-2}) were converted to photoisomerizations (Rh*) using the collecting area estimated for each rod from trial-to-trial variability in the responses to a fixed-strength flash. Assuming Poisson fluctuations in photon absorption dominated response variability, the mean number of Rh* produced by the flash was estimated by dividing the square of the mean response by the variance. This procedure was repeated for three or four flash strengths to estimate each rod's collecting area.

Spatially restricted stimuli were delivered through an adjustable slit (Cairn Research Ltd., Kent, UK) and focused on the cell through a 60× microscope objective (Nikon, Kanagawa, Japan; 0.95 NA). The nominal width of the slit was <1 μm. Broadening due to diffraction in the optics was estimated by imaging a small fluorescent bead (30 nm; Molecular Probes, Eugene, OR) through the same objective used to deliver local illumination. The image of a bead inside a suction electrode had a full width at half maximum of ~0.5 μm. This indicated that light delivered through the slit was restricted to a <2 μm region of the outer segment. Although this calibration procedure could have underestimated the width of the illuminated region, our conclusions from these experiments were not changed by moderate increases in the width of illumination. Each absorbed photon will spread to a region of the outer segment at least 1.25 μm wide, with complete saturation occurring for the minimum spatial spread. In the case of complete saturation, the near-linear scaling of responses to 1–3 photons in Figure 3C could be explained only if the illuminated region was >6 μm wide. Thus the response linearity indicated a lack of local saturation rather than spatial spread of the local illumination.

Data Analysis

Fits to Histograms of Response Amplitudes

The amplitudes of responses to a repeated dim flash (e.g., Figure 1B) were measured from the correlation between individual responses and the normalized average response. This procedure rejects noise except that with temporal characteristics like the single photon response. The correlation was measured over the initial 250–300 ms of the response, which includes the rising phase and peak but not the recovery. Restricting the amplitude estimates to this time window provided the cleanest separation of single photon responses and failures.

Amplitude histograms were fit to identify responses to 0 or 1 Rh*. Fits assumed that the number of photons absorbed per trial was described by Poisson statistics and that the dark noise and noise in the single photon response were independent and additive. In this case, the number of responses with an amplitude between $A - \Delta A/2$ and $A + \Delta A/2$ is

$$N(A) = \Delta A \sum_{n=0}^{\infty} \frac{\exp(-\bar{n})\bar{n}^n}{n!} [2\pi(\sigma_D^2 + n\sigma_A^2)]^{-1/2} \times \exp\left(-\frac{(A - n\bar{A})^2}{2(\sigma_D^2 + n\sigma_A^2)}\right) \quad (1)$$

Here $\bar{A}$ is the mean single photon response amplitude and σ_A is its standard deviation, n is the number of Rh* produced by the flash and $\bar{n}$ is its mean, and σ_D is the standard deviation of the current fluctuations in darkness. To provide accurate estimates of these parameters, we simultaneously fit histograms measured for 2–4 flash strengths to find a common $\bar{A}$ and σ_A; $\bar{n}$ was determined from the cell's collecting area and the flash strength and σ_D was determined from fits to sections of record in darkness. The average values of $\sigma_D/\bar{A}$ from fits to the amplitude histograms were 0.22 and 0.25 for primate and guinea pig rods; similarly, the average values of $\sigma_A/\bar{A}$ were 0.24 and 0.20.

The fit parameters were used to set thresholds to isolate responses contributing to the singles and failures peaks in the amplitude histogram. These thresholds were set at $3\bar{A}/2$ and near $\bar{A}/2$ (somewhat lower if σ_D was small). All responses smaller than the lower threshold were identified as failures. Responses between the lower threshold and upper threshold were identified as singles.

Contamination of Singles and Failures

The lack of dependence of the amplitude of the isolated singles and failures on flash strength (Figures 1D and 1E) provided a bound on the extent of contamination. To estimate this bound, we generated distributions of putative rod responses for several flash strengths according to Equation 1 and set thresholds to identify singles and failures. We then determined how the average amplitude of the identified responses depended on flash strength. Increasing the dark noise, σ_D, or variability in the single photon response, σ_A, caused the average amplitude to depend more strongly on flash strength than observed. Values of $\sigma_D/\bar{A}$ or $\sigma_A/\bar{A}$ greater than 0.25 were inconsistent with the confidence interval for the slope of the best-fit line through the points in Figure 1E. These values of σ_D and σ_A and the thresholds used to identify responses produce about 10% contamination of the isolated singles and omission of 10% of the actual single photon responses. This provided an upper bound to the errors in isolation.

The thresholds used to identify singles represent a compromise between minimizing contamination and omitting single photon responses. To estimate how much the omitted responses might affect the estimated response variability, we altered the thresholds to increase contamination while decreasing the number of omitted responses. When the thresholds were positioned such that at most 5% of the singles were omitted, the coefficient of variation of the response areas increased by 15%. Furthermore, the late time-to-peak and broad temporal width of the time-dependent variance still held and multistep shutoff still provided the best explanation of the response fluctuations. Thus our conclusions were relatively insensitive to changes in the criteria used to isolate responses.

Phototransduction Cascade Model

We tested three classes of models for how the single photon response is regulated. Each consisted of a stochastic model of rhodopsin's activity followed by a deterministic model for the remainder of the transduction cascade. The action of the transduction cascade was approximated as a linear filter applied to the time course of rhodopsin's activity (Figure 9B).

We assumed that rhodopsin's activity, on average, decayed exponentially with a 200 ms time constant. The rate constants describing rhodopsin's effective catalytic activity in each model (Figures 4A–4C and associated text) were adjusted accordingly. This slow decay of rhodopsin's activity is required if variations in rhodopsin's activity are to explain the increase in response variability during the response recovery (Figure 2). A much faster decay of rhodopsin's activity (<150 ms) caused the responses to vary in amplitude but

not shape. A substantially slower decay (>300 ms) is inconsistent with other measurements (Calvert et al., 2001). For each model, the time course of the activity of a single rhodopsin molecule was generated numerically.

The form of the transduction cascade filter was determined from a linear approximation to the biochemical reactions that make up the cascade (Rieke and Baylor, 1998b). The Fourier transform of the resulting filter $F(t)$ is

$$\tilde{F}(\omega) = \frac{G_D}{[\phi - i\omega][P_D + 12\beta^2 P_D/(\beta^2 + \omega^2) - i\omega(1 - 12\beta P_D/(\beta^2 + \omega^2))]}, \quad (2)$$

where ω is the temporal frequency in radians/s, G_D is the dark cGMP concentration, ϕ is the rate constant for the decay of PDE activity, β is the rate constant for removal of Ca^{2+} from the outer segment by Na^+/K^+, Ca^{2+} exchange (Nakatani and Yau, 1988; Cervetto et al., 1989), P_D is the dark PDE activity, and $\tilde{F}(\omega) = \int dt \exp(i\omega t)F(t)$. Equation 2 assumes that Ca^{2+} stimulation of the rate of cGMP synthesis operates with a cooperativity of 4 (Koch and Stryer, 1988; Burns et al., 2002).

The filter in Equation 2 depends on two time scales: (1) that governing the decay of PDE activity following rhodopsin shutoff; and (2) that governing the replenishment of the cGMP concentration by synthesis, including the feedback action of Ca^{2+}. G_D was determined from the measured dark current, I_D, assuming $I_D = k\,G_D^3$ with $k = 8 \times 10^{-3}$ pA/μM^3 (Rieke and Baylor, 1996). β was determined by fitting the Na^+/K^+, Ca^{2+} exchange current with a single exponential (Figure 9C). For modeling control responses, β was set equal to the average measured exchange rate. P_D and ϕ were adjusted to obtain a good fit to the time course of the average single photon response. Predictions for primate rods used the following parameters: $\beta = 25\ s^{-1}$, $G_D = 15\ \mu M$, $P_D = 1.4\ s^{-1}$, and $\phi = 5\ s^{-1}$. Predictions for guinea pig rods used: $\beta = 20\ s^{-1}$, $G_D = 13.5\ \mu M$, $P_D = 1.8\ s^{-1}$, and $\phi = 8\ s^{-1}$.

In the experiments of Figure 6, we loaded cells with the calcium buffer BAPTA. To predict the resulting change in response, we measured the rate constant for Na^+/K^+, Ca^{2+} exchange in the presence of BAPTA (Figure 9C) and adjusted β in Equation 2 accordingly. All other parameters in the filter were held constant. Figure 9B shows impulse responses of the transduction cascade in control and BAPTA-loaded conditions and the predicted change in the current response.

The qualitative differences between the different models for reproducibility illustrated in Figure 5 depended on the characteristics of rhodopsin shutoff but not the model for the transduction cascade. Thus the parameters in Equation 2 could be increased or decreased by a factor of 2 without changing the conclusions reached in Results. The inability of feedback to account for the observed time course of the variance held for both the model described above and the model of Nikonov et al. (1998).

Acknowledgments

We thank Denis Baylor, Peter Detwiler, Bertil Hille, and A.P. Sampath for comments on the manuscript; Dennis Dacey, Matt McMahon, and Orin Packer for help with primate tissue; and Eric Martinson and Maria McKinley for excellent technical assistance. Support was provided by the NIH through grant EY-11850 and by the McKnight Foundation.

Received: April 10, 2002
Revised: July 9, 2002

References

Arshavsky, V.Y., Lamb, T.D., and Pugh, E.N., Jr. (2002). G proteins and phototransduction. Annu. Rev. Physiol. *64*, 153–187.

Baylor, D.A., Lamb, T.D., and Yau, K.-W. (1979a). The membrane current of single rod outer segments. J. Physiol. *288*, 589–612.

Baylor, D.A., Lamb, T.D., and Yau, K.-W. (1979b). Responses of retinal rods to single photons. J. Physiol. *288*, 613–634.

Baylor, D.A., Matthews, G., and Yau, K.-W. (1980). Two components of electrical dark noise in toad retinal rod outer segments. J. Physiol. *309*, 591–621.

Baylor, D.A., Nunn, B.J., and Schnapf, J.L. (1984). The photocurrent, noise and spectral sensitivity of rods of the monkey *Macaca fascicularis*. J. Physiol. *357*, 575–607.

Bennett, N., and Sitaramayya, A. (1988). Inactivation of photoexcited rhodopsin in retinal rods: the roles of rhodopsin kinase and 48-kDa protein (arrestin). Biochemistry *27*, 1710–1715.

Berg, H.C., and Purcell, E.M. (1977). Physics of chemoreception. Biophys. J. *20*, 193–219.

Bialek, W. (1987). Physical limits to sensation and perception. Annu. Rev. Biophys. Biophys. Chem. *16*, 455–478.

Bohm, S.K., Grady, E.F., and Bunnett, N.W. (1997). Regulatory mechanisms that modulate signalling by G-protein-coupled receptors. Biochem. J. *15*, 1–18.

Burns, M.E., Mendez, A., Chen, J., and Baylor, D.A. (2002). Dynamics of cyclic GMP synthesis in retinal rods. Neuron, in press.

Calvert, P.D., Govardovskii, V.I., Krasnoperova, N., Anderson, R.E., Lem, J., and Makino, C.L. (2001). Membrane protein diffusion sets the speed of rod phototransduction. Nature *411*, 90–94.

Cervetto, L., Lagnado, L., Perry, R.J., Robinson, D.W., and McNaughton, P.A. (1989). Extrusion of calcium from rod outer segments is driven by both sodium and potassium gradients. Nature *337*, 740–743.

Chen, J., Makino, C.L., Peachey, N.S., Baylor, D.A., and Simon, M.I. (1995). Mechanisms of rhodopsin inactivation in vivo as revealed by a COOH-terminal truncation mutant. Science *267*, 374–377.

Detwiler, P.B., Ramanathan, S., Sengupta, A., and Shraiman, B.I. (2000). Engineering aspects of enzymatic signal transduction: photoreceptors in the retina. Biophys. J. *79*, 2801–2817.

DeVries, H., and Stuiver, M. (1961). The absolute sensitivity of the human sense of smell. In Principles of Sensory Communication, W.A. Rosenblith, ed. (Cambridge, MA: MIT Press), pp. 159–167.

Dohlman, H.G. (2002). G proteins and pheromone signaling. Annu. Rev. Physiol. *64*, 129–152.

Felber, S., Breuer, H.P., Petruccione, F., Honerkamp, J., and Hofmann, K.P. (1996). Stochastic simulation of the transducin GTPase cycle. Biophys. J. *71*, 3051–3063.

Field, G.D., and Rieke, F. (2002). Nonlinear signal transfer from mouse rods to bipolar cells and implications for visual sensitivity. Neuron *34*, 773–785.

Firestein, S. (2001). How the olfactory system makes sense of scents. Nature *413*, 211–218.

Gibson, S.K., Parkes, J.H., and Liebman, P.A. (2000). Phosphorylation modulates the affinity of light-activated rhodopsin for G protein and arrestin. Biochemistry *39*, 5738–5749.

Hecht, S., Shlaer, S., and Pirenne, M. (1942). Energy, quanta and vision. J. Gen. Physiol. *25*, 819–840.

Hille, B.H. 2001. Ion Channels of Excitable Membranes, 3rd ed. (Sunderland, MA: Sinauer Associates, Inc.).

Koch, K.W., and Stryer, L. (1988). Highly cooperative feedback control of retinal rod guanylate cyclase by calcium ions. Nature *334*, 64–66.

Leinders-Zufall, T., Lane, A.P., Puche, A.C., Ma, W., Novotny, M.V., Shipley, M.T., and Zufall, F. (2000). Ultrasensitive pheromone detection by mammalian vomeronasal neurons. Nature *405*, 792–796.

Leskov, I.B., Klenchin, V.A., Handy, J.W., Whitlock, G.G., Govardovskii, V.I., Bownds, M.D., Lamb, T.D., Pugh, E.N., Jr., and Arshavsky, V.Y. (2000). The gain of rod phototransduction: reconciliation of biochemical and electrophysiological measurements. Neuron *27*, 525–537.

Matthews, H.R. (1991). Incorporation of chelator into guinea-pig rods shows that calcium mediates mammalian photoreceptor light adaptation. J. Physiol. *436*, 93–105.

Mendez, A., Burns, M.E., Roca, A., Lem, J., Wu, L.W., Simon, M.I., Baylor, D.A., and Chen, J. (2000). Rapid and reproducible deactivation of rhodopsin requires multiple phosphorylation sites. Neuron *28*, 153–164.

Mendez, A., Burns, M.E., Sokal, I., Dizhoor, A.M., Baehr, W., Palczewski, K., Baylor, D.A., and Chen, J. (2001). Role of guanylate cyclase-activating proteins (GCAPs) in setting the flash sensitivity of rod photoreceptors. Proc. Natl. Acad. Sci. USA *98*, 9948–9953.

Menini, A., Picco, C., and Firestein, S. (1995). Quantal-like current fluctuations induced by odorants in olfactory receptor cells. Nature *373*, 435–437.

Nakatani, K., and Yau, K.-W. (1988). Calcium and magnesium fluxes across the plasma membrane of the toad rod outer segment. J. Physiol. *395*, 695–729.

Nikonov, S., Engheta, N., and Pugh, E.N., Jr. (1998). Kinetics of recovery of the dark-adapted salamander rod photoresponse. J. Gen. Physiol. *111*, 7–37.

Palczewski, K., Rispoli, G., and Detwiler, P.B. (1992). The influence of arrestin (48K protein) and rhodopsin kinase on visual transduction. Neuron *8*, 117–126.

Rieke, F., and Baylor, D.A. (1996). Molecular origin of continuous dark noise in rod photoreceptors. Biophys. J. *71*, 2553–2572.

Rieke, F., and Baylor, D.A. (1998a). Single-photon detection by rod cells of the retina. Rev. Mod. Phys. *70*, 1027–1036.

Rieke, F., and Baylor, D.A. (1998b). Origin of reproducibility in the responses of retinal rods to single photons. Biophys. J. *75*, 1836–1857.

Sakitt, B. (1972). Counting every quantum. J. Physiol. *223*, 131–150.

Vuong, T.M., Chabre, M., and Stryer, L. (1984). Millisecond activation of transducin in the cyclic nucleotide cascade of vision. Nature *311*, 659–661.

Whitlock, G.G., and Lamb, T.D. (1999). Variability in the time course of single photon responses from toad rods: termination of rhodopsin's activity. Neuron *23*, 337–351.

Wilden, U., and Kühn, H. (1982). Light-dependent phosphorylation of rhodopsin: number of phosphorylation sites. Biochemistry *21*, 3014–3022.

Xu, J., Dodd, R.L., Makino, C.L., Simon, M.I., Baylor, D.A., and Chen, J. (1997). Prolonged photoresponses in transgenic mouse rods lacking arrestin. Nature *389*, 505–509.